Magneto-optics of a charge-tunable quantum dot: Observation of a negative diamagnetic shift

G. Peniakov [1,2,*] A. Beck [1,†] E. Poem [3,†] Z.-E. Su [1] B. Taitler [1] S. Höfling [2] G. W. Bryant [4,5] and D. Gershoni [1]

[1]*The Physics Department and the Solid State Institute, Technion–Israel Institute of Technology, Haifa 3200003, Israel*

[2]*Julius-Maximilians-Universität Würzburg, Physikalisches Institut, Lehrstuhl für Technische Physik, Am Hubland, 97074 Würzburg, Germany*

[3]*Department of Physics of Complex Systems, Weizmann Institute of Science, Rehovot 7610001, Israel*

[4]*Nanoscale Device Characterization Division, National Institute of Standards and Technology, Gaithersburg, Maryland 20899, USA*

[5]*Joint Quantum Institute, National Institute of Standards and Technology and University of Maryland, College Park, Maryland 20742, USA*

(Received 4 December 2022; revised 20 February 2025; accepted 25 February 2025; published 17 March 2025)

We present magneto-optical studies of a self-assembled semiconductor quantum dot in neutral and positively charged states. The diamagnetic shifts and Zeeman splitting of many well-identified optical transitions are precisely measured. Remarkably, a pronounced negative diamagnetic shift is observed for spectral lines resulting from a doubly positively charged excitonic complex. We use the Hartree-Fock approximation for describing the direct Coulomb and exchange interactions between the quantum dot confined carriers in various configurations. A simple harmonic potential model, which we extend to capture the influence of an externally applied magnetic field in Faraday configuration, is then used to quantitatively account for all the measured diamagnetic shifts. We show that the negative shift is due to the change in the hole-hole exchange interaction energy induced by the magnetic field. Using this model and the measured shifts we extract the dielectric constant of the quantum dot material and get a decent estimate of the quantum dot dimensions. Further, the measured Zeeman splitting of the various spectral lines are also explained by a simple model using algebraic sums and differences of the g factors of the confined charge carriers in their respective first and second discrete energy levels. Finally, the obtained values of the electronic g factor and that of the dielectric constant are independently used to determine the effective composition (x) of the ternary $In_xGa_{1-x}As$ quantum dot. Both agree to within the experimental uncertainties.

DOI: 10.1103/PhysRevB.111.115306

I. INTRODUCTION

Self-assembled quantum dots (QDs) in semiconductors form a well-known platform for quantum technologies. They have proven to be the best contemporary single-photon sources [1–5], while providing an excellent interface between anchored spin qubits and "flying" photon qubits [6]. Much progress has been made in controlling confined-spin qubits in QDs [7–10], entangling them with photons [11–16], and allowing deterministic generation of long strings of entangled photons [17–19]. In addition, QDs still provide a convenient platform for studying many-body complexes composed of multiple confined carriers. Interesting properties of such complexes include the relative interactions between the constituent particles, the form of their spatial wave functions, and their response to externally applied fields. In particular, an externally applied magnetic field removes the Kramers' degeneracy and causes the optical transitions to energetically shift. The first interaction, known as the Zeeman-interaction, depends linearly on the field strength, while the second interaction known as the *diamagnetic shift*, depends quadratically on the field strength [20]. Modeling these shifts in confined systems and in particular in semiconductor nanostructures is still a subject of many research efforts [21–25].

We present here a magneto-optical study, mainly in Faraday configuration, of a semiconductor QD with very well-identified optical transitions between various few-confined-carriers configuration in different charge states. In particular, we focus our attention on the magneto optical properties of the doubly, positively charged excitonic complex X^{+2}.

The X^{+2} can be intuitively described as a confined multicarrier configuration containing three heavy holes and one electron. After a radiative recombination of an electron-hole pair, the QD remains with two holes, one in the lowest energy level and one in the second level. These two holes may form either three spin triplet states or one spin singlet state. Our work was spurred by noticing an anomaly in the diamagnetic shifts of the optical transitions into the singlet state, labeled $X^{+2}_{S_0}$, which we found to be **negative**. In the effort of understanding this phenomenon, we found that the X^{+2} excitonic transitions form an excellent platform for studying the electron-hole and hole-hole exchange interactions and their dependence on an externally applied magnetic field. Using the Hartree-Fock approximation and a simple two-dimensional (2D), cylindrically symmetric, harmonic-oscillator model for describing the QD spatial potential, we quantitatively describe all the measured diamagnetic shifts and in turn determine the QD's average dielectric constant and its dimensions. In

*Contact author: giora.peniakov@uni-wuerzburg.de
†These authors contributed equally to this work.

addition, from the measured Zeeman splittings of the various spectral lines we determine the electron and hole g factors in their respective two lowest discrete energy levels. We show that the heavy hole g factor switches sign between the first and second confined levels.

Finally, we show that both the obtained dielectric constant and the electron g factor provide a way to estimate the $In_xGa_{1-x}As$ QD's average composition (x).

The paper is organized as follows. In Sec. II, we briefly describe the experimental system. In Sec. III we present full polarization-sensitive magneto-PL measurements displaying the diamagnetic shifts and Zeeman splitting of many well-identified optical transitions and their polarization selection rules. We provide a simple model to explain the measured Zeeman splittings of the spectral lines and present in particular the anomalous negative diamagnetic shift of the doubly positively charged exciton, the $X^{+2}_{S_0}$. In Sec. IV we discuss in detail the theoretical model that we use to analyze the measured magneto-optics data and in Sec. V we compare the model predictions and the measured results.

II. EXPERIMENTAL SYSTEM

We studied a single $In_xGa_{1-x}As$ self-assembled QD embedded in a planar microcavity grown along the [001] direction. The actual dimensions of the studied QD, about 35 nm in diameter and 3–4 nm in height, were estimated from a set of detailed optical studies and comparisons with many-carrier model simulations [26]. These structural characterizations were also backed by atomistic simulations [27]. We used an Attocube [28] closed-cycle cryostat to cool the sample down to 4 K. A built-in vector magnet enabled the application of a magnetic field in any desired direction. The emitted photoluminescence (PL) was collected by a $\times 60$ objective. Its polarization was analyzed by pairs of liquid crystal variable retarders and polarizing beam splitters, enabling PL polarization projection on any direction in the Poincaré sphere. The PL was then spectrally analyzed using an 80 cm double monochromator, providing spectral resolution of $\sim$20 μeV.

The QD was optically excited using an above band-gap continuous wave red HeNe laser or a blue diode laser, emitting at 633 or 445 nm, respectively. The excitation color affects the average charge state of the QD. While red HeNe illumination results in positive charging, blue diode laser excitation leads to neutral or negative charging [26].

We define the symmetry axis of the QD and the optical beam path as the z direction. The x and y axes are defined along the polarization eigenstates of the QD's bright exciton (BE), X^0_{BE}, as explained below.

III. RESULTS

A. Neutral bright and dark excitons

The X^0_{BE} is an electron-hole pair which can be expressed in the spin basis $\{|+z\rangle = |\Uparrow\downarrow\rangle, |-z\rangle = |\Downarrow\uparrow\rangle\}$ with $\Uparrow\Downarrow$ and $\uparrow\downarrow$ denoting the spin projections of the heavy-hole and electron onto the z axis. Since a heavy-hole and an electron have total angular momenta of 3/2 and 1/2, respectively, the angular momentum projection of a $|\Uparrow\downarrow\rangle$ ($|\Downarrow\uparrow\rangle$) pair along this axis is $+1$ (-1) [29]. Consequently, optical recombination of the $|\Uparrow\downarrow\rangle$ and $|\Downarrow\uparrow\rangle$ pairs results in a right-handed (R) and left-handed (L) circularly polarized photon emission, respectively.

The anisotropic electron-hole exchange interaction in this QD lifts the degeneracy of the above basis by $\delta_1^{e1h} \approx 30\,\mu\mathrm{eV}$ [30] thus forming new eigenstates $\sqrt{2}|\psi_{\mathrm{BE}}\rangle_{s,as} = \sqrt{2}|\pm x\rangle = |\Uparrow\downarrow\rangle \pm |\Downarrow\uparrow\rangle$, where the subscript s (as) stands for symmetric (antisymmetric) spin wave functions. Recombination of those excitonic eigenstates results in either horizontal, $\sqrt{2}H = R + L$, or vertical $\sqrt{2}V = i(R - L)$ rectilinearly polarized photon emission, enabling a one-to-one correspondence between the X^0_{BE}'s two-level system and the photon's polarization [30]. We use the cross-rectilinearly polarized components of the X^0_{BE} spectral lines for defining the x and y axes of our experimental system.

The dark exciton (DE), X^0_{DE}, is another electron-hole pair state, but with parallel spins $\sqrt{2}|\psi_{\mathrm{DE}}\rangle_{s,as} = |\Uparrow\uparrow\rangle \pm |\Downarrow\downarrow\rangle$. In general, the X^0_{DE} is optically inactive [10], however, small optical activity of the X^0_{DE} was measured [31–33]. Zielinski *et al.* attributed this activity to a small mixing of the X^0_{DE} and X^0_{BE} eigenstates induced by symmetry reduction of the QD potential [32]. This naturally occurred mixing is rather small [10] but can be enhanced by externally applying in-plane magnetic field perpendicular to the optical z axis (Voigt configuration). For a magnetic field direction parallel to the z axis (Faraday configuration) no additional mixing is expected, thus the X^0_{DE} remains optically inactive [34].

The Zeeman interaction between an externally applied magnetic field and QD confined carriers' spin removes the Kramers' degeneracy between the confined carriers spin state. The eigenstates are usually the parallel and antiparallel spin directions relative to the direction of the magnetic field. The Zeeman interaction depends linearly on the magnetic field magnitude. This dependence is most generally expressed in terms of a 3×3 g-factor tensor [35]. For simplicity, we assume here that this tensor is diagonal and have only two different components: along the symmetry axis (g_e^z and g_h^z) and perpendicular to it ($g_e^\perp$ and $g_h^\perp$) [36]. Thus in Faraday configuration the Zeeman splitting is given by Eq. (1):

$$\mathcal{H} = -\mu_B g_e^z B_z S_z + \tfrac{1}{3}\mu_B g_h^z B_z J_z. \tag{1}$$

Here, μ_B is the Bohr magneton, S_z and J_z are the angular momentum z projections $\pm\frac{1}{2}$ and $\pm\frac{3}{2}$, of the confined electron and heavy hole respectively and B_z is the magnitude of the magnetic field.

In the first part of the experiment, we measured the confined electron and hole g factors tensor components along the z axis. This was done by measuring the Zeeman splitting of the X^0_{BE} and X^0_{DE} under B field in the $\hat{z}$ direction. Assuming that the absolute magnitude of the g factors of those transitions are given by the sum and difference of the absolute magnitudes of the single-carrier g factors

$$\left|g^z_{\mathrm{BE(DE)}}\right| = \left|g^z_e\right| \pm \left|g^z_h\right| \tag{2}$$

[37,38], we were able to extract g_e^z and g_h^z from the measured g^z_{BE} and g^z_{DE} [34,36,39]. Equation (2) is derived from the parallel and antiparallel spin nature of the DE and BE, using the sign convention given by the Zeeman Hamiltonian Eq. (1).

If one takes into account also the excitonic fine structure due to the electron-hole exchange interaction, the BE and DE

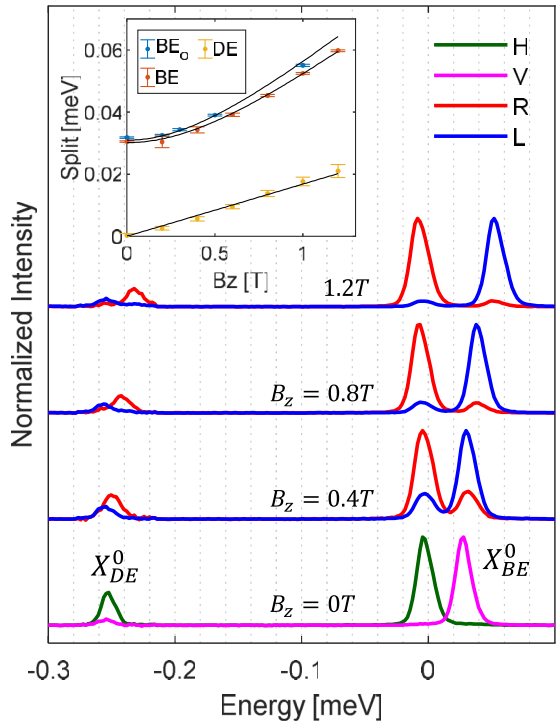

FIG. 1. Polarization-sensitive magneto-PL of the bright and dark excitons ($X^0_{\rm BE}$ and $X^0_{\rm DE}$), for various magnetic field strengths. The magnetic field has two components, one in the $\hat{z}$ direction which we vary, and one which is fixed ($1.5T$) in $\hat{x}$ direction. The resulting Zeeman splittings are summarized in the Inset for both excitons using yellow (DE) and brown (BE) data points. Blue data points in the Inset represent measurements of the BE splittings without the $\hat{x}$ field component. The errorbars represent the experimental uncertainties due to the finite spectral resolution of the measurements. Solid black lines represent best fits to Eq. (3), by which the g factors are extracted.

Zeeman splitting is given by [34]

$$\Delta E_{\rm BE(DE)} = \sqrt{\left(\delta^{1e1h}_{1,2}\right)^2 + \left(\mu_B g^z_{\rm BE(DE)} B_z\right)^2}, \qquad (3)$$

where $\delta^{1e1h}_{1,2}$ are the fine-structure splittings of the $X^0_{\rm BE}$ and $X^0_{\rm DE}$ at 0 field, respectively.

In Fig. 1, we present polarization sensitive PL spectra of the QD neutral excitons under various magnetic field strengths in Faraday configuration (z direction). To increase the visibility of the DE we added during these measurements an in-plane magnetic field of 1.5 T. In the inset to Fig. 1 the measured Zeeman splittings of the DE and BE as a function of the B_z field strength deduced from these measurements are displayed as yellow and brown data points, respectively, overlaid by solid black lines representing best fit of Eq. (3). To estimate the influence of the in-plane magnetic field on the measured Zeeman interaction we repeated the measurements of the BE in the absence of the in-plane field [blue data points and best fitted Eq. (3) in the inset to Fig. 1]. The deduced g factor of the BE with and without the in-plane field is -0.74 and -0.81, respectively. This small difference (less than 10%) sets an upper bound on the possible error in the measured g factor of the DE. Moreover, we note that in the absence of B_z, the DE measured splittings is negligible, setting even a lower bound on the possible error in the value that we measure. This should not come as a surprise, since the electron and hole in-plane g factors (which we measured in a separate experiment) are much smaller than those in the Faraday direction [36].

TABLE I. Measured excitonic fine structure splittings and g-factor tensor z components. Here $\delta^{1e1h}_{1,2}$ is the bright (dark) exciton line splitting at $B = 0$, and $g^z_{(e/h)}$ are the g factors of the electron and hole in Faraday configuration, respectively.

Spectral line	$\delta^{1e1h}_{1,2}$[μeV]	g^z factor	Model
$X^0_{\rm BE}$	31(2)	−0.81(2)	$g^z_{1e} + g^z_{1h}$
$X^0_{\rm DE}$	1.4(1)*	−0.29(4)	$g^z_{1e} - g^z_{1h}$

$g^z_{1e} = -0.55(4)$; $g^z_{1h} = -0.26(4)$; $\delta^{1e1h}_0 = 270(10)$ μeV

*The $X^0_{\rm DE}$ zero-field splittings δ^{1e1h}_2 is too small to be directly resolved here. It was measured using time-resolved spectroscopy in Ref. [10]. δ^{1e1h}_0 denotes the measured $X^0_{\rm BE}$-$X^0_{\rm DE}$ zero-field splittings.

One also notices in Fig. 1 that the $X^0_{\rm DE}$ cross-polarized doublet is not equally intense: at 0 field, its horizontally (H) polarized component is much stronger than the vertically (V) polarized one, a phenomenon observed and explained in previous publications [10,27,40]. Adding magnetic field in Faraday configuration enhances the weaker component and gradually increases the cross-circular polarization components of the the $X^0_{\rm DE}$ doublet. However, up to the maximal field strength of 1.5 T, the two $X^0_{\rm DE}$'s components remain unequal. Nonetheless, we extracted the g factors of the $X^0_{\rm BE}$ and $X^0_{\rm DE}$ by fitting their measured Zeeman splittings to Eq. (3). Table I summarizes the values of the measured excitonic g factors, and the deduced single-carrier g factors extracted from a simple arithmetic model, $g^z_{\rm BE(DE)} = g^z_{1e} \pm g^z_{1h}$.

B. Diamagnetic shifts

In Fig. 2, we present a full set of Magneto-PL measurements in Faraday configuration of the QD. We present the PL spectra for two average charge states of the QD: negative and positive. The QD average charge state is apparent in each case by considering the emission ratio between the positive and negative trions, X^+ and X^-. Many identified lines are marked in the PL following previous studies [26].

All the observed spectral lines split into two components under the application of external magnetic field along the optical axis z. At high fields the two components are mostly cross-circularly polarized as can be seen in the lowest panel of Fig. 2. The line splitting is known to be due to the Zeeman interaction between the confined carriers and the external magnetic field as expressed in Eq. (1).

On top of the splitting due to the Zeeman interaction, the spectral lines undergo a clear quadratic-in-B (diamagnetic) shift. This shift is well described for all the measured magneto photo-luminescence lines by adding a term βB^2 to the Hamiltonian [Eq. (1)]. This term faithfully describes the experimentally measured shifts for all the spectral lines as shown in Fig. 2. The diamagnetic shift refers to the spectral "center of mass," defined as $E(B) = (E_R(B) + E_L(B))/2$, where E_R and E_L are the energies of the two Zeeman components emitting

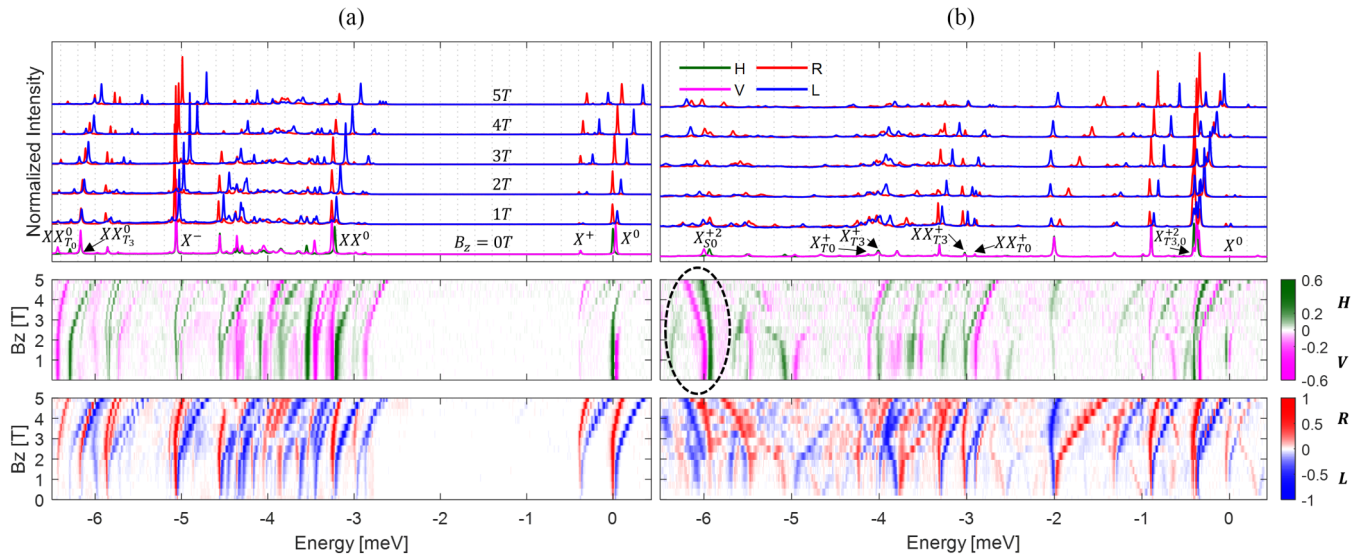

FIG. 2. Polarization-sensitive magneto-PL spectra in Faraday configuration for various magnetic field strengths, for negatively (a) and positively (b) charged QD. The upper panel shows polarization-sensitive magneto-PL spectra. The panels below show the degree of circular and rectilinear polarizations, given by the color bars to the right, as a function of the photon energy and the externally applied magnetic field strength. The identified spectral lines are marked: X^0 and XX^0, the neutral bright exciton and biexciton, and $XX^0_{T_0(T_3)}$, the neutral metastable biexcitons with the two holes in $T_0(T_3)$ spin triplet configurations. The X^+ (X^-) positively (negatively) charged trion, $X^+_{T_0(T_3)}$, and $XX^+_{T_0(T_3)}$ are similar positively charged excitons and biexcitons. The X^{+2} lines result from the recombination of the doubly positively charged exciton, leaving behind two holes that can form either a singlet S_0 or one of the triplets, $T_{\pm 3}$ or T_0. Note the negative diamagnetic shift of the $X^{+2}_{S_0}$ (marked with an oval dash line). The energy scale is relative to the X^0_{BE} spectral line at zero magnetic field. The X^0_{BE} spectral line is clearly observed when the QD is statistically closed to neutrality (a), but the line is suppressed when the QD is strongly positively charged (b).

in cross circular R and L polarizations, respectively. In most cases, $E(B)$ shifts toward higher energy (hence, the terminology of "diamagnetic" versus "paramagnetic" shift). Figure 3 summarizes the diamagnetic shifts of several selected lines. One can see that many lines, including the XX^0 and the trions, X^- and X^+, exhibit similar diamagnetic shifts to that of the BE ($\sim 8\,\mu\mathrm{eV}/T^2$).

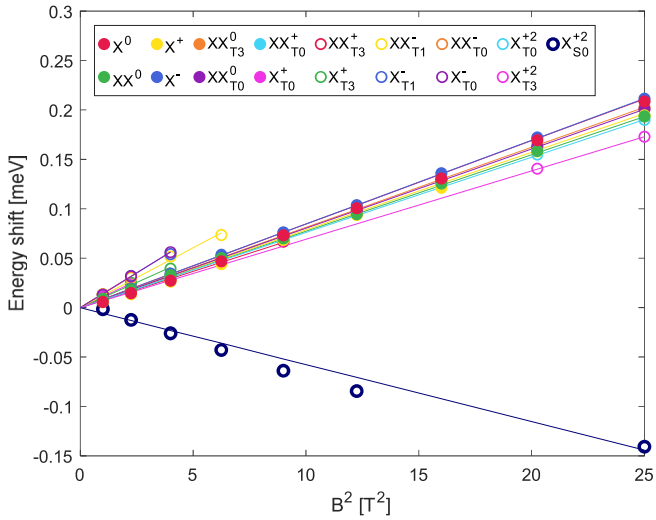

FIG. 3. Measured energy shifts of various optical transitions as a function of B^2. The $X^{+2}_{S_0}$ spectral line is a prominent exception—it shows a negative diamagnetic shift.

C. Diamagnetic shifts of the X^{+2} spectral lines

Interestingly, a few spectral lines in Fig. 2(b) when the QD is positively charged shift toward lower energy as the external field increases. In particular, one prominent spectral line at -5.95 meV (at zero field) exhibits such a distinctive *negative* diamagnetic shift. We focus our discussion on this particular line (represented by the blue circles in Fig. 3). We identify this line as the doubly charged exciton transition $X^{+2}_{S_0}$, where the subscript S_0 refers to the singlet configuration of the two holes in the final state of this transition. The other triplet configurations of the final states result in the three optical transitions at about -0.38 meV. We denote them by $X^{+2}_{T_0}$ and $X^{+2}_{T_{\pm 3}}$. These spectral lines are presented on an expanded energy scale in Fig. 4. The other less prominent lines which also exhibit negative shifts result from two-hole singlet states in which the second hole is in a higher level than the second hole-level. Since the thermal population of these higher energy initial levels is lower, these lines are weaker. For the sake of simplicity, they will not be further discussed in this work.

The identification of the spectral lines follows Ref. [26], where the same QD was studied. The identifications are based on the following arguments. (i) these spectral lines appear in the spectrum only when the QD is strongly positively charged, like in Fig. 2(b). (ii) the $X^{+2}_{S_0}$ and $X^{+2}_{T_0}$ transitions exhibit the same fine-structure splitting of $\sim 70\,\mu\mathrm{eV}$ due to the same splitting in their initial state, denoted δ_1^{1e2h} (see detailed energy level scheme in Fig. 5). (iii) The energy difference between these states is ~ 5 meV, matching previously measured hole-hole exchange interaction energies, for example, between the excited positive trion states $(1e^1)(1h^12h^1)_S$

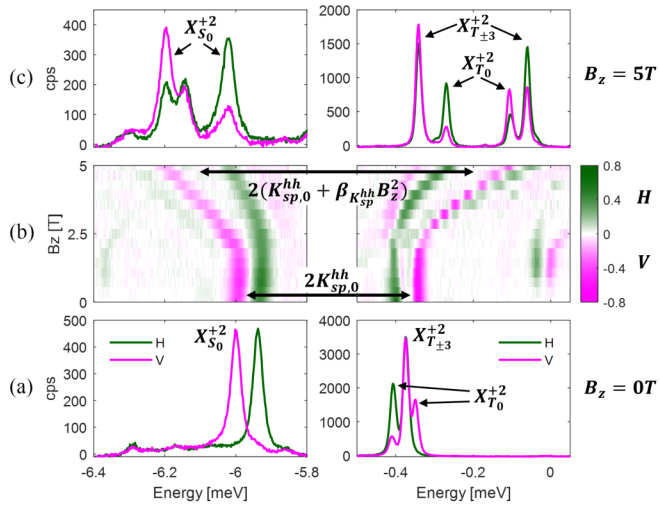

FIG. 4. Rectilinear polarization-sensitive PL spectra of the X^{+2} spectral lines relative to the neutral exciton state (a) at zero magnetic field, (b) as function of the externally applied field in Faraday configuration, and (c) in magnetic field of $5T$. The transitions are marked by their final spin configurations (S_0, T_0, $T_{\pm3}$). The energy difference between the $X^{+2}_{T_0}$ and the $X^{+2}_{S_0}$ doublets (marked) equals twice the hole-hole exchange interaction $K^{hh}_{sp,0}$.

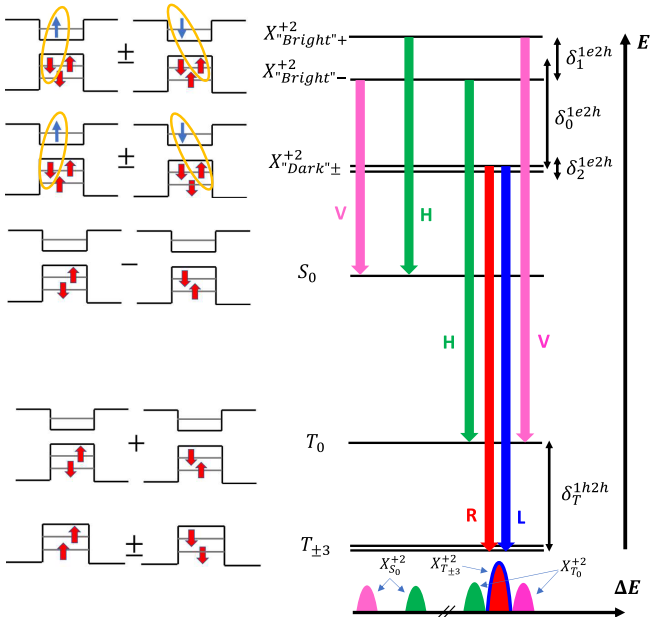

FIG. 5. Schematic description of the energy levels and optical transitions associated with the doubly positively charged exciton X^{+2}. The configuration of each state is presented on the left, where thin blue arrows represent electrons with spin $\frac{1}{2}$, and thick arrows represent heavy-holes with spin $\frac{3}{2}$. The polarization selection rules are marked by colored downward arrows. H (V) marks the horizontal (vertical) rectilinear polarization, while R (L) marks the circular right-handed (left-handed) polarization. A schematic description of the emitted PL is drawn at the bottom. The $X^{+2}_{T_{\pm3}}$ spectral line is drawn in red with a blue edge, symbolizing that the R and L polarizations overlap such that the emission is unpolarized.

and $(1e^1)(1h^12h^1)_T$, or between the positive biexciton states $(1e^2)(1h^22h^1)$ [26]. Here, np^m reads: n, the energy level order; p, the particle type (e or h); and m, the number of particles occupying this level (either one or two). The subscript of parentheses that includes two carriers of the same type, describes their mutual spin configuration—either a singlet, S_0, or triplet, T_l, where $l = 0, \pm1$ for two electrons or $0, \pm3$ for two heavy-holes, denotes the total spin projection on the z axis.

Figure 5 schematically describes the energy levels and the optical transitions associated with the doubly charged exciton, X^{+2}. This exciton comprises one electron in the ground-level $1e^1$, and three holes: two of them forming a singlet in the s-shell ground-level, $1h^2$, and the third one occupies the first excited p-shell level $2h^1$. The exchange interaction between the Pauli-unpaired electron (in the 1st level) and the Pauli-unpaired hole (in the second level) removes the degeneracy between the four possible two-carriers' spin configurations, forming four distinct eigenstates similar to the case of the neutral exciton (X^0). As such, we borrow the exciton "bright" and "dark" terminology to describe the eigenstates of the X^{+2} as well. States with antiparallel e-h spins are called "brightlike," while states with parallel spins—"darklike" (see Fig. 5). We emphasize that the dark and bright states are both optically active since the optical recombination occurs mostly between the unpaired s electron and one of the s-level singlet holes, rather than with the unpaired p hole. The $1e^1$-$2h^1$ recombination is very inefficient (about two orders of magnitude weaker [10]) since it is forbidden by symmetry.

The final states of the X^{+2} recombination contain two holes—one in the ground level and one in the first excited level. As identical particles, they form either one singlet spin state denoted by S_0^{1h2h} or three triplet states denoted by $\{T_0^{1h2h}, T_{\pm3}^{1h2h}\}$, respectively. The two initial bright-like exciton states can only recombine to the singlet S_0^{1h2h} or triplet T_0^{1h2h} final states (but not to the $T_{\pm3}^{1h2h}$), resulting in two pairs of cross-rectilinearly polarized doublets [41]; the darklike states can only recombine to the $T_{\pm3}^{1h2h}$ states. Because in the absence of external magnetic field the darklike states and the $T_{\pm3}^{1h2h}$ states are each nearly degenerate, the recombination results in a single, unpolarized, strong spectral line. We label the X^{+2} optical transitions by their final states, specified in their subscripts: $X^{+2}_{T_0}$, $X^{+2}_{T_{\pm3}}$ and $X^{+2}_{S_0}$. The latter transition, $X^{+2}_{S_0}$, is the one exhibiting a negative diamagnetic shift. We note that in the absence of external field, the unpolarized $X^{+2}_{T_{\pm3}}$ spectral line is positioned exactly in between the two cross linearly polarized components of the $X^{+2}_{T_0}$ line. This indicates that δ_0^{1e2h}, denoting the splitting between the darklike and brightlike X^{+2} states, is equal to δ_T^{1h2h}, the splitting between the holes' triplet states T_0^{1h2h} and $T_{\pm3}^{1h2h}$.

A detailed polarization-sensitive magneto-PL spectra of the X^{+2} spectral lines are presented in Fig. 4. One can see that while the triplet lines shift toward higher energy with increasing B field, the singlet lines shift toward lower energy. Since the initial states of the $X^{+2}_{S_0}$ and $X^{+2}_{T_0}$ transitions are the same (the brightlike exciton states), we conclude that the sign difference between the diamagnetic shifts of the two transitions stems from the different influence that the external magnetic field has on the final states. The h-h singlet final state rises in energy faster than the initial state such that the overall

TABLE II. *g* factors and zero-field splitting (ZFS) of the charged excitons spectral lines transitions, compared to those of the neutral excitons. The measured splittings are explained by a simple model which assumes that the *g* factor of a given transition can be decomposed to the sum of the comprising charge carrier *g* factors of the initial and final states of the optical transition. $g^z_{n(e/h)}$ denotes the *g* factor of the electron (hole) in the *n* energy level of the QD, where $n = 1$ is the ground level.

Spectral line	ZFS [μeV]	*g* factor	Model
X^0_{BE}	31(2)	−0.81(2)	$g^z_{1e} + g^z_{1h}$
X^+	0	−0.81(2)	
X^-	0	−0.94(2)	
$X^{+2}_{T_{\pm 3}}$	0	−0.97(5)	
$X^{+2}_{T_0}$	56(2)	0.55(10)	$g^z_{1e} + g^z_{2h}$
$X^{+2}_{S_0}$	69(7)	0.65(7)	
$g^z_{2h} = 1.15(12)$; $\delta_0^{1e2h} = 130(10)\,\mu\mathrm{eV}$			

spectral shift is negative (red shift). However, the *h*-*h* triplet state rises in energy slower than the initial state, thus the total spectral shift is positive (blue shift).

D. Measured *g* factors of the charged excitons $X^{\pm 1}$ and X^{+2}

The measured *g* factors of the charged excitons $X^{\pm}$, and X^{+2} optical transitions are summarized in Table II together with that of the neutral bright exciton X^0. In discussing these *g* factors, one should consider the Zeeman interaction both in the initial and in the final states of the optical transitions. For example, in the initial state of the $X^{\pm}$ exciton the unpaired electron (hole) interacts with the field while in the final state the remaining hole (electron) interacts with the field. Thus, like in the case of the BE, one expects that the measured spectral line *g* factor is a sum of the electron and hole *s*-level *g* factors. Similarly, the final states of the brightlike X^{+2} transitions are either the two-holes T_0 triplet or S_0 singlet states. Both states have zero *g* factors, since they are nondegenerate and their total angular momentum projection on the magnetic field direction vanishes. Therefore, the *g* factors of these transitions are due to the initial brightlike exciton state only. This state contains a Pauli-unpaired electron in the first *s* level and a Pauli-unpaired hole in the second *p* level. The two paired holes occupying the ground level singlet state do not contribute to the Zeeman interaction with an externally applied magnetic field. Thus, the measured *g* factors of the $X^{+2}_{T_0}$ and $X^{+2}_{S_0}$ lines are expected to be the same. In addition, like the BE, their zero-field splitting is given by the anisotropic electron-hole exchange term δ_1^{1e2h}. The overall *g* factor of this transition is therefore:

$$(E^{\mathrm{initial}} - E^{\mathrm{final}})/(\mu_B B_z) = g^z_{1e} - \left(-g^z_{2h}\right) = g^z_{1e} + g^z_{2h}. \quad (4)$$

The extra minus sign results from the optical selection rule stating that only an electron and a hole with antiparallel spins can radiatively recombine.

The lines *g* factors are extracted by fitting their measured Zeeman splittings to Eq. (3). Table II summarizes the extracted values. The results of this simple arithmetic calculation are presented in the "Model" column of Table II. Comparing this simple model with experiments, one indeed finds that the measured *g* factors of spectral lines like X^+, X^-, and other optical transitions whose *g*-factor arithmetics produces the sum of the electron and hole ground level *g* factors, are similar to the measured value of the BE [42,43]. The same arithmetic shows that *g* factor of the doubly charged exciton triplet states $X^{+2}_{T_{\pm 3}}$ is yet another example. However, the *g* factors of the $X^{+2}_{S_0}$ and $X^{+2}_{T_0}$ transitions are similar to those that include the *g* factor of the hole in its second energy level (g^z_{2h}) rather then the first (g^z_{1h}) [42,43]. It is interesting to note that it follows (see Table II) that $g^z_{2h} = 1.15 \pm 0.10$. This value is opposite in sign compared to the ground level *g* factors of the hole and that of the electron [−0.26 and −0.55, respectively (see Table I)]. The opposite sign of the excited-hole *g* factor was directly measured on another similar QD sample using PLE spectroscopy [43]. This finding is also supported by realistic NextNano [28] simulations [42]. Similar results of sign difference between the first and second confined levels were observed and discussed for electrons and holes in quantum wells [20,44].

IV. THEORETICAL ANALYSIS

A. Hartree-Fock approximation applied to QD-confined multicarrier configurations

We use the Hartree-Fock approximation [45] for describing the multicarrier configurations involved in the various initial and final states of the optical transitions that we study. In this approximation, the many-body state is a single Slater determinant of single-particle states. The single-particle states are found as confined states in the dot, described by a parabolic model-potential, in the strong-confinement limit where any possible single-particle reshaping by interaction with the other particles is ignored. One expresses the energies of the many-body states as sums of single-particle energies, plus the direct Coulomb and exchange interactions between all pairs of particles in the particular configuration.

For example, the energy of the neutral bright (BE) and dark (DE) excitons are given by

$$E_{X^0_{\mathrm{BE}}} = E^e_s + E^h_s - J^{eh}_{ss}, \quad (5)$$

and

$$E_{X^0_{\mathrm{DE}}} = E^e_s + E^h_s - J^{eh}_{ss} - 2K^{eh}_{ss} = E_{X^0_{\mathrm{BE}}} - 2K^{eh}_{ss}, \quad (6)$$

where $E^{e(h)}_s$ is the confinement energy of the electron (hole) in the *s* level and J^{eh}_{ss} ($K^{eh}_{ss} = 0.5\delta_0^{1e1h}$) is the direct Coulomb (exchange) interaction between the electron and the hole. We note here that as a rule, one subtracts twice the exchange energy when the spins of the two particles are aligned [45]. This rule applies also for the case of electron and hole pair though they are distinguishable quasiparticles [46,47]. The electron-hole anisotropic exchange interactions, δ_1^{1e1h} (δ_2^{1e1h}) which removes the degeneracy between the bright (dark) exciton eigenstates is usually much smaller than δ_0^{1e1h} [29], and does not affect the excitonic transitions' spectral center of gravity. Therefore, we ignore these, as well as δ_1^{1e2h} (δ_2^{1e2h}) in this discussion.

Applying the same rules to the positively charged exciton, the X^{+1}, in which the initial state is formed from two holes in

their respective s-level and one electron is in its respective s level, one gets

$$E_{X^{+1}}^{\text{initial}} = E_s^e + 2E_s^h - 2J_{ss}^{eh} - 2K_{ss}^{eh} + J_{ss}^{hh}. \tag{7}$$

After the electron-hole recombination, the final state contains only one hole in its s level

$$E_{X^{+1}}^{\text{final}} = E_s^h. \tag{8}$$

The optical transition energy is therefore

$$\begin{aligned} E_{X^{+1}} &= E_{X^{+1}}^{\text{initial}} - E_{X^{+1}}^{\text{final}} = E_s^e + E_s^h - 2J_{ss}^{eh} - 2K_{ss}^{eh} + J_{ss}^{hh} \\ &= E_{X_{\text{DE}}^0} + J_{ss}^{hh} - J_{ss}^{eh}. \end{aligned} \tag{9}$$

It turns out, that the energy difference between the X^{+1} and the X_{DE}^0 transitions is given by the difference between the two direct Coulomb terms on the right hand side of Eq. (9).

We proceed by applying the same rules to the doubly positively charged exciton, the X^{+2} spectral lines. Considering first the energies of the initial states,

$$\begin{aligned} E_{X_{S_0}^{+2}}^{\text{initial}} = E_{X_{T_0}^{+2}}^{\text{initial}} &= E_s^e + 2E_s^h + E_p^h + J_{ss}^{hh} + 2J_{sp}^{hh} \\ &\quad - 2J_{ss}^{eh} - J_{sp}^{eh} - 2K_{ss}^{eh} - 2K_{sp}^{hh}, \end{aligned} \tag{10}$$

$$E_{X_{T_{\pm 3}}^{+2}}^{\text{initial}} = E_{X_{T_0}^{+2}}^{\text{initial}} - 2K_{sp}^{eh}, \tag{11}$$

and then of the final states,

$$E_{X_{S_0}^{+2}}^{\text{final}} = E_s^h + E_p^h + J_{sp}^{hh}, \tag{12}$$

$$E_{X_{T_0}^{+2}}^{\text{final}} = E_{X_{T_{\pm 3}}^{+2}}^{\text{final}} = E_s^h + E_p^h + J_{sp}^{hh} - 2K_{sp}^{hh}. \tag{13}$$

We note that here as well we subtract twice the exchange energy whenever a pair of particles has parallel spins.

The transition energies are then given as before by the differences between the initial and final states,

$$E_{X_{T_0}^{+2}} = E_{X^{+1}} + J_{sp}^{hh} - J_{sp}^{eh}, \tag{14}$$

$$E_{X_{S_0}^{+2}} = E_{X_{T_0}^{+2}} - 2K_{sp}^{hh}, \tag{15}$$

$$E_{X_{T_{\pm 3}}^{+2}} = E_{X_{T_0}^{+2}} - 2K_{sp}^{eh}, \tag{16}$$

where we also used Eq. (9). It follows that the energy difference between the X^{+1} spectral line and the $X_{T_0}^{+2}$ spectral line is given by the difference between the two direct Coulomb terms J_{sp}^{hh} and J_{sp}^{eh}.

B. Two-dimensional parabolic potential model

To quantitatively compare our model [Eqs. (6), (9), (14), (15), and (16)] with the measured PL spectra, we proceed with a model for calculating the direct Coulomb and exchange interactions. We follow Warburton *et al.* [48] who developed a simple two-dimensional, cylindrically symmetric, harmonic oscillator model for describing the QD confining potential for charge carriers. In their model, the harmonic potential is described by two parameters: $\omega_{e(h)}$, the harmonic frequency of the confining potential and $m_{e(h)}$, the in-plane effective mass, for each one of the confined carriers, the electron (e) or the heavy hole (h), respectively. The effective length of the potential l_p is related to the effective mass and frequency by

$$l_p = \sqrt{\frac{\hbar}{m_p \omega_p}}, \tag{17}$$

where l_p is the effective length for particle type $p \in \{e, h\}$.

The single particle wave functions for the two lowest energy levels in this model are

$$\Psi^{1p}(\rho) = \frac{1}{\sqrt{\pi} l_p} e^{-\frac{\rho^2}{2l_p^2}}; \quad \Psi_{\pm 1}^{2p}(\rho, \phi) = \frac{\rho}{\sqrt{\pi} l_p^2} e^{\left(-\frac{\rho^2}{2l_p^2} \pm i\phi\right)}, \tag{18}$$

where ρ and ϕ are the conventional inplane particle's radius vector length and polar angle, respectively.

The various direct Coulomb interaction integrals, $J_{ij}^{p_i p_j}$, where i, j indicate the confined carriers' states and p_i, p_j indicate their types, can be thus analytically calculated [48]. Relevant to our discussion, as discussed above, are the direct and exchange terms between holes and electrons in their respective lowest two energy levels "s and p shells." Interactions between particles of the same type are inversely proportional to l_p [48],

$$J_{ss}^{pp} = \frac{4}{3} J_{sp}^{pp} = 4K_{sp}^{pp} = \frac{\alpha}{l_p}, \tag{19}$$

with

$$\alpha = \sqrt{\frac{\pi}{2}} \frac{e^2}{4\pi \epsilon_0 \epsilon_r}. \tag{20}$$

Here e is the electron charge, ϵ_0 is the vacuum permittivity, and ϵ_r is the relative permittivity (dielectric constant) of the QD material.

In a similar way the direct Coulomb interactions between carriers of different types are given by

$$J_{ss}^{pp'} = \alpha \left(\frac{2}{l_p^2 + l_{p'}^2} \right)^{\frac{1}{2}}; \quad J_{sp}^{pp'} = \frac{\alpha}{\sqrt{2}} \frac{2l_p^2 + l_{p'}^2}{\left(l_p^2 + l_{p'}^2\right)^{\frac{3}{2}}}. \tag{21}$$

Since the electron and the hole are distinguishable quasiparticles [46,47] the exchange terms K_{ss}^{eh} and K_{sp}^{eh} are not directly given by the Hartree Fock model. Yet, since these exchange terms are known to be mainly short range they can be approximated by [20,46]

$$K_{ij}^{eh} \approx E_{sr}^{eh} a_0^3 \int \left| f_{ij}^X(\mathbf{r}, \mathbf{r}) \right|^2 d\mathbf{r}, \tag{22}$$

where E_{sr}^{eh} is the short-range electron-hole exchange interaction, a_0 is the crystal lattice constant [20,46] and $f_{i,j}^X(\mathbf{r_e}, \mathbf{r_h})$ is the envelope function of the exciton formed by electron in the i level and hole in the j level. We proceed by approximating the exciton envelope functions as a product of the single carrier envelope functions $f_{i,j}^X(\mathbf{r_e}, \mathbf{r_h}) \approx \Psi^{ie}(\boldsymbol{r_e}) \Psi^{jh}(\boldsymbol{r_h})$. This approximation is valid for QDs in which the confining potential is larger than the electron hole direct Coulomb interaction.

Hence,

$$K_{ss}^{eh} \approx E_{sr}^{eh} a_0^2 \int |\Psi^{1e}(\boldsymbol{\rho})|^2 |\Psi^{1h}(\boldsymbol{\rho})|^2 d\boldsymbol{\rho} = \frac{E_{sr}^{eh} a_0^2}{l_e^2 + l_h^2}, \quad (23)$$

$$K_{sp}^{eh} \approx E_{sr}^{eh} a_0^2 \int |\Psi^{1e}(\boldsymbol{\rho})|^2 |\Psi^{2h}(\boldsymbol{\rho})|^2 d\boldsymbol{\rho} = \frac{E_{sr}^{eh} a_0^2 l_e^2}{\left(l_e^2 + l_h^2\right)^2}, \quad (24)$$

where we used in Eqs. (23) and (24) the corresponding single carrier envelope functions from Eq. (18) .

The ratio between these exchange terms is therefore given by

$$\frac{K_{sp}^{eh}}{K_{ss}^{eh}} = \frac{l_e^2}{l_e^2 + l_h^2} = \frac{\gamma^2}{1+\gamma^2}, \quad (25)$$

where we define the ratio between the characteristic lengths of the carriers' potential: $\gamma = \frac{l_e}{l_h}$.

Experimentally, as we show below for the QD under study, it turns out that l_e and l_h are nearly equal and $\gamma \approx 1$. Therefore by substituting $\gamma = 1 + \eta$, with $|\eta| \ll 1$ in Eq. (25) and keeping only leading terms in η, one gets that

$$\frac{K_{sp}^{eh}}{K_{ss}^{eh}} \approx \frac{1}{2}(1+\eta) \approx \frac{1}{2}. \quad (26)$$

In a similar way one gets for the direct Coulomb and same particle exchange terms that

$$J_{ss}^{hh} - J_{ss}^{eh} = 4\left(J_{sp}^{hh} - J_{sp}^{eh}\right) \approx \tfrac{1}{2}\eta J_{ss}^{hh} = 2\eta K_{sp}^{hh}. \quad (27)$$

In addition, it is worth noting that the direct Coulomb attraction between the electron and the hole in their respective lowest energy levels J_{ss}^{eh} can be used as an estimate for the BE binding energy E_{BE}. Thus, using Eqs. (27) and (19), we get

$$E_{\mathrm{BE}} \approx J_{ss}^{eh} \approx J_{ss}^{hh}\left(1 - \tfrac{1}{2}\eta\right) = 4K_{sp}^{hh}\left(1 - \tfrac{1}{2}\eta\right). \quad (28)$$

Equations (25), (27), and (28) are useful since, as we show below, the hole-hole and electron-hole exchange energies K_{sp}^{hh}, K_{sp}^{eh}, and η can be determined experimentally from the PL spectra at zero external magnetic field.

C. Magnetic field dependence of the direct and exchange Coulomb interactions

To include the effect of the magnetic field in this model, we replace ω_p with $\omega_p(B) \equiv \sqrt{\omega_p^2 + \frac{e^2B^2}{4m_p^2}}$, obtained by adding a magnetic field Hamiltonian to the harmonic oscillator one and solving for the eigenenergies (harmonic spectrum plus Landau levels spectrum). Using Eq. (17) the expression for the effective length then becomes

$$l_p(B) = l_{p,0}\left[1 + \left(\frac{el_{p,0}^2}{2\hbar}\right)^2 B^2\right]^{-\frac{1}{4}}, \quad (29)$$

where we add the subscript "0" (such as in $l_{p,0}$) to indicate the value in the absence of magnetic field.

In low magnetic fields, the magnetic energy is much smaller than the confinement energy, such that $(\frac{el_{p,0}^2}{2\hbar})^2 B^2 \ll 1$, and to lowest terms in B:

$$l_p(B) \approx l_{p,0}\left[1 - \left(\frac{el_{p,0}^2}{4\hbar}\right)^2 B^2\right]. \quad (30)$$

Since by Eq. (19), $K_{sp,0}^{pp}$ is inversely proportional to $l_{p,0}$, it follows from Eq. (30) that the field dependence of the exchange energy can be approximated by

$$K_{sp}^{pp}(B) \approx K_{sp,0}^{pp} + \beta_{K_{sp}^{pp}} B^2, \quad (31)$$

where

$$\beta_{K_{sp}^{pp}} = K_{sp,0}^{pp}\left(\frac{el_{p,0}^2}{4\hbar}\right)^2 \quad (32)$$

is the diamagnetic shift coefficient of the same particle (hole-hole or electron-electron) exchange interaction.

Using Eqs. (19) and (20), one obtains an expression for the value of the particle-particle exchange diamagnetic shift coefficient, $\beta_{K_{sp}^{pp}}$:

$$\beta_{K_{sp}^{pp}} = \frac{e^{10}}{2^{22}\pi^2\hbar^2\epsilon_0^4\epsilon_r^4\left(K_{sp,0}^{pp}\right)^3}. \quad (33)$$

Equation (33) is important, since both the hole-hole exchange interaction $K_{sp,0}^{hh}$ and its diamagnetic shift $\beta_{K_{sp}^{hh}}$ can be directly deduced from our measurements, providing thus a way to uniquely determine ϵ_r.

Since by Eq. (30) the field dependence of the effective hole and electron lengths are different, γ and η are also field dependent:

$$\gamma(B) = \frac{l_e(B)}{l_h(B)} \approx \gamma_0\left[1 + \left(1 - \gamma_0^4\right)\left(\frac{el_{h,0}^2}{4\hbar}\right)^2 B^2\right], \quad (34)$$

where γ_0 and $l_{h,0}$ are defined in the absence of magnetic field and we keep only lowest order terms in B. Using $\eta_0 = \gamma_0 - 1$, keeping only first-order terms in η_0 one gets

$$\eta(B) = \eta_0\left[1 - 4\left(\frac{el_{h,0}^2}{4\hbar}\right)^2 B^2\right]. \quad (35)$$

Therefore, the field dependence of the product $\eta \times K_{sp}^{hh}$ up to lowest order terms in B, used in Eqs. (27) and (28) is given by

$$\eta(B) \times K_{sp}^{hh}(B) \approx \eta_0 K_{sp,0}^{hh} - 3\eta_0\beta_{K_{sp}^{hh}} B^2. \quad (36)$$

To conclude this section, we note that from the measured hole-hole exchange term $K_{sp,0}^{hh}$ and its diamagnetic shift $\beta_{K_{sp}^{hh}}$, one can straightforwardly calculate, using Eq. (32), the extent of the hole parabolic confining potential $l_{h,0}$. Then, by using Eq. (23), the intrinsic short-range electron hole exchange term E_{sr}^{eh}, can be estimated as well. Together with the measured value of η_0, as we show below, the diamagnetic shifts of practically all the measured optical transitions, can be estimated.

D. Magnetic field dependence of the electron-hole exchange terms

The isotropic electron-hole exchange term, K_{ss}^{eh}, which equals half of the DE-BE fine structure splitting (δ_0^{1e1h},

Table I) is, as mentioned above, mostly due to the short-range exchange interaction [20,46]. Its dependence on the magnetic field results as shown in Eq. (23) from its inverse dependence on the term $(l_h^2 + l_e^2) = l_h^2(1+\gamma^2) \approx 2l_h^2(1+\eta)$ (or roughly twice the QD area [46]). Therefore, by using the field dependence of l_h [Eq. (30)] and that of η [Eq. (35)] in Eq. (23), while keeping only lowest terms in B^2 and η_0 one obtains

$$K^{eh}_{ss(p)}(B) = K^{eh}_{ss(p),0} + \beta_{K^{eh}_{ss(p)}} B^2, \tag{37}$$

where

$$\beta_{K^{eh}_{ss}} = 2(1+2\eta_0)\frac{K^{eh}_{ss,0}}{K^{hh}_{sp,0}}\beta_{K^{hh}_{sp}} \tag{38}$$

and

$$\beta_{K^{eh}_{sp}} = 2\frac{K^{eh}_{sp,0}}{K^{hh}_{sp,0}}\beta_{K^{hh}_{sp}}, \tag{39}$$

where we also used Eq. (32).

Equations (38) and (39) relate the field dependence of the electron-hole exchange to the hole-hole exchange and thus provide a way for estimating the magnetic field dependencies of the electron hole exchange interactions. We use these relations to compare the model estimate with the actually measured diamagnetic shifts.

E. Diamagnetic shifts of the bright and dark excitons

The diamagnetic shift of the free exciton is proportional to its wave-function area [20] in a plane normal to the direction of the magnetic field:

$$\beta_{X^0_{\rm BE}} = \frac{e^2}{8\mu}\langle f|\hat{\rho_{\rm ex}}^2|f\rangle. \tag{40}$$

Here, $\rho_{\rm ex} = \rho_e - \rho_h$ is the relative radius vector between the electron and hole, $f(\rho_{ex})$ is the excitonic envelope wave function, and $\mu = m_e m_h/(m_e+m_h)$ is the reduced mass of the electron and hole.

For a confined exciton the effect of the geometric confinement potential on the exciton center of mass is approximated by anisotropic deformation of the exciton wave function $f(\rho_{\rm ex})$, which is taken to be a hydrogenic-like ellipsoid of revolution, characterized by effective anisotropic Bohr radii parallel to its three principal axes. Equivalently, since the Bohr radii are inversely proportional to the reduced mass, one uses in this approximation three direction-dependent reduced exciton masses ($\mu_i, i = x, y, z$). For such an asymmetric hydrogenic wave function, the diamagnetic shift in Faraday configuration, with magnetic field along z, is given by first-order perturbation theory [49,50] as

$$\beta_{X^0_{\rm BE}} = \frac{4\pi^2\hbar^4\epsilon_0^2\epsilon_r^2}{e^2\mu\mu_x\mu_y}, \quad \frac{1}{\mu} = \frac{1}{3}\left(\frac{1}{\mu_x}+\frac{1}{\mu_y}+\frac{1}{\mu_z}\right). \tag{41}$$

While the excitonic binding energy at zero magnetic field is given by the regular Rydberg formula:

$$E_{\rm BE} = \frac{e^4\mu}{32\pi^2\hbar^2\epsilon_0^2\epsilon_r^2}. \tag{42}$$

After the exciton recombination, the QD remains empty of carriers. This final "vaccum" state does not shift with the magnetic field and therefore the measured diamagnetic shift of the BE transition is positive and given by Eq. (41).

TABLE III. Measured and modeled diamagnetic shifts (β values) in $\mu eV/T^2$. The estimated relative errors are about 5%. For the model we used the zero field measured $K^{hh}_{sp,0} = 2.79(15)$ meV [Eq. (46)], $K^{eh}_{ss,0} = 0.5\delta^{11}_0 = 0.135(7)$ meV (Table I) and $\eta_0 = -0.024(3)$ [Eq. (50)].

	Measured	Calculated	Theoretical expression
$\beta_{X^0_{\rm BE}}$	8.44	8.44	Eq. (45) ($\chi = 1.36$)
$\beta_{X^0_{\rm DE}}$	7.0	7.2	$\beta_{X^0_{\rm BE}} - 2\beta_{K^{eh}_{ss}}$
β_{X^+}	7.85	7.95	$\beta_{X^0_{\rm DE}} - 6\eta_0\beta_{K^{hh}_{sp}}$
$\beta_{X^{+2}_{T_0}}$	7.6	8.09	$\beta_{X^+} - \frac{3}{2}\eta_0\beta_{K^{hh}_{sp}}$
$\beta_{X^{+2}_{S_0}}$	−5.8	−5.6	$\beta_{X^{+2}_{T_0}} - 2\beta_{K^{hh}_{sp}}$
$\beta_{X^{+2}_{T_{\pm 3}}}$	6.9	6.9	$\beta_{X^{+2}_{T_0}} - 2\beta_{K^{eh}_{sp}}$
$\beta_{K^{hh}_{sp}}$	6.7	6.7	Eq. (33) ($\epsilon_r = 14.24$)
$\beta_{K^{eh}_{ss}}$	0.62	0.62	Eq. (38)
$\beta_{K^{eh}_{sp}}$	0.55	0.35	Eq. (39)

In our circularly symmetric QD model, $\mu_x = \mu_y = \mu_{xy}$ and $\mu_z = \frac{\mu_{xy}}{a}$, where $a = l_z/l_{xy}$ is the aspect ratio between the normal and lateral dimensions of the QD confined excitonic wave function. One can therefore express $\mu = \chi\mu_{xy}$, where $\chi = \frac{3}{2+a}$. In the 2D limit $a = 0$, $\mu_z = \infty$, and $\chi = 3/2$.

Using Eqs. (41) and (42) one can now express the excitonic diamagnetic shift in terms of the excitonic binding energy:

$$\beta_{X^0_{\rm BE}} = \frac{\chi^2 e^{10}}{2^{13}\pi^4\hbar^2\epsilon_0^4\epsilon_r^4}\frac{1}{E^3_{\rm BE}}. \tag{43}$$

From Eq. (6) and the quadratic field dependence of all the direct Coulomb and exchange terms it immediately follows that

$$\beta_{X^0_{\rm DE}} = \beta_{X^0_{\rm BE}} - 2\beta_{K^{eh}_{ss}}. \tag{44}$$

In a similar way one can calculate the expected diamagnetic shifts of the charged excitons as well (see Table III).

To conclude this section we note that Eq. (43) much resembles Eq. (33). In fact, if one uses $J^{eh}_{ss} = (4-2\eta_0)K^{hh}_{sp,0}$ [Eq. (28)] as an estimate for the excitonic binding energy ($E_{\rm BE}$), then the ratio between the diamagnetic shifts of the hole-hole exchange interaction and that of the bright exciton depends only on the geometrical ratios χ and η_0:

$$\left(\frac{\beta_{X^0_{\rm BE}}}{\beta_{K^{hh}_{sp}}}\right) \approx \frac{8\chi^2}{\pi^2(1-6\eta_0)}; \lim_{\chi,\eta_0 \longrightarrow \frac{3}{2},0}\left(\frac{\beta_{X^0}}{\beta_{K^{hh}_{sp}}}\right) = 2\left(\frac{3}{\pi}\right)^2. \tag{45}$$

Surprisingly, for equally confined electron and hole in the 2D limit, the model predicts a universal ratio which is independent of the QD dimensions and material properties.

V. DISCUSSION

A. Estimating the hole-hole and electron-hole exchange terms

The exchange terms can now be estimated directly from the measured PL spectrum of the quantum dot.

From Eq. (15) it directly follows that

$$K^{hh}_{sp,0} = \left(E_{X^{+2}_{T_0}} - E_{X^{+2}_{S_0}}\right)\Big/2 = 2.79(15)\,\text{meV}, \quad (46)$$

[see Figs. 2(b) and 4]. From Eq. (6) it follows that

$$K^{eh}_{ss,0} = \left(E_{X^0_{\text{BE}}} - E_{X^0_{\text{DE}}}\right)\Big/2 = 0.135(5)\,\text{meV}, \quad (47)$$

(see Fig. 1). From Eq. (22) one expects that $K^{eh}_{sp,0} = 0.5K^{eh}_{ss,0} \approx 63(5)\,\mu\text{eV}$. This result should be compared with Eq. (16) from which it follows that $K^{eh}_{sp,0} = (E_{X^{+2}_{T_0}} - E_{X^{+2}_{T_3}})/2 \approx 0(20)\,\mu\text{eV}$ [see Figs. 2(b) and 4]. Unfortunately, there is a small discrepancy here, probably because of the lack of spectral resolution, due to the spectral lines' widths and a possible degeneracy removal between the T_0 and $T_{\pm 3}$ two-heavy-hole triplet states [51], which our model does not take into account.

From Eq. (9) it follows that

$$J^{hh}_{ss} - J^{eh}_{ss} = E_{X^{+1}} - E_{X^0_{\text{DE}}} = -130(15)\,\mu\text{eV}. \quad (48)$$

[see Figs. 1 and 2(a)]. Likewise, from Eqs. (14),

$$J^{hh}_{sp} - J^{eh}_{sp} = E_{X^{+2}_{T_0}} - E_{X^{+1}} = -30(15)\,\mu\text{eV} \quad (49)$$

[see Figs. 2(a) and 4], which within the limited resolution of our measurements agrees well with the expected ratio of 1:4 between $J^{hh}_{sp} - J^{eh}_{sp}$ and $J^{hh}_{ss} - J^{eh}_{ss}$, following Eq. (27).

We proceed by using Eqs. (19) and (27) to get an estimate for η_0:

$$\eta_0 = \left(J^{hh}_{ss} - J^{eh}_{ss}\right)/2K^{hh}_{sp,0} = -0.024(3). \quad (50)$$

Likewise, using Eq. (28) we get an estimate for the binding energy of the BE:

$$E_{\text{BE}} \approx J^{eh}_{ss} \approx 4K^{hh}_{sp,0}\left(1 - \tfrac{1}{2}\eta_0\right) = 11.3(4)\,\text{meV}. \quad (51)$$

B. Measured and estimated diamagnetic shifts

The measured diamagnetic shifts are summarized in the second column of Table III. The diamagnetic shifts of the spectral lines are displayed in the upper six rows of the table. From these measurements, we directly obtain the measured diamagnetic shifts of the hole-hole and electron-hole exchange terms: Using Eq. (15) we get

$$\beta_{K^{hh}_{sp}} = \left(\beta_{X^{+2}_{T_0}} - \beta_{X^{+2}_{S_0}}\right)\Big/2, \quad (52)$$

using Eq. (44) we get

$$\beta_{K^{eh}_{ss}} = \left(\beta_{X^0_{\text{BE}}} - \beta_{X^0_{\text{BE}}}\right)\Big/2, \quad (53)$$

and using Eq. (16) we get

$$\beta_{K^{eh}_{sp}} = \left(\beta_{E_{X^{+2}_{T_0}}} - \beta_{E_{X^{+2}_{T_{\pm 3}}}}\right)\Big/2. \quad (54)$$

The obtained values are also listed in the last three rows of Table III.

The calculated diamagnetic shifts are displayed for comparison in the third column of Table III. The expressions used for these calculations were developed in Sec. IV using the Hartree-Fock approximation and the cylindrical parabolic potential model for the QD, are displayed and referenced in the fourth column of the table. As one can see, the agreement is surprisingly decent, despite the simplicity of our model for the QD potential and despite the fact that the Hartree-Fock model completely ignores the correlation terms in the Coulombic interactions [52] and we do not include any single-particle reshaping that occurs from interaction.

TABLE IV. The estimated average composition of the QD estimated from the deduced dielectric constant and the measured electronic g factor. The dielectric constant and band parameters are interpolated using Eq. (55) and the tabulated parameters.

	GaAs	InAs	Bowing	Best x	$In_xGa_{1-x}As$
ϵ_r	15.15[a]	12.46[a]	0.67[b]	0.71	14.24
E_p[eV]	28.8[c]	21.1[c]	−1.48[c]	0.76	23.22
E_g[eV]	1.519[c]	0.418[c]	2.22[c]	0.76	1.295[*]
Δ[eV]	0.341[c]	0.39[c]	0.15[c]	0.76	0.351
g_e Calculated	−0.317	−14.3		0.76	−0.55
g_e Measured	−0.484[d]	−14.9[d]			−0.55

[*]The measured excitonic emission+excitonic binding energy (see text).
[a]Ref. [53].
[b]Ref. [54].
[c]Ref. [55].
[d]Ref. [20].

C. QD dielectric constant and average composition

By substituting the measured $K^{hh}_{sp,0}$ and $\beta_{K^{hh}_{sp}}$ in Eq. (33) we find that the average dielectric constant of the QD is $\epsilon_r = 14.24(4)$. This experimentally deduced value provides a way to estimate the QD effective composition. Since the QD comprises two binary semiconductors, GaAs and InAs, one may interpolate the value of any material property (Q) of the ternary material using an average effective composition x for the QD ternary material $In_xGa_{1-x}As$ using quadratic interpolation formula

$$Q(x) = xQ^{In} + (1-x)Q^{Ga} - c^Q x(1-x), \quad (55)$$

where Q^{In} (Q^{Ga}) is the Q value of the binary material InAs (GaAs) and C^Q is a bowing parameter characterizing Q for the ternary material. The material parameters that we use for the dielectric constants are given in Table IV, in which we list and reference the relevant input parameters for the quadratic interpolations used in this work.

The effective QD composition which results in the experimentally deduced dielectric constant is $x = 0.70 \pm 0.05$. Interestingly, similar value for x is obtained if one interpolates the measured electronic QD g factor.

The isotropic electronic g factor in bulk semiconductors can be analytically calculated by the Roth's formula [56]:

$$g_e = 2 - \frac{2}{3}\frac{E_p\Delta}{E_g(E_g+\Delta)}, \quad (56)$$

where E_g is the band gap energy between the valence and conduction bands, Δ is the split-off gap (between the valence band and the spin-orbit band) at $k = 0$, and E_p is the Kane energy defined as $E_p \equiv \frac{2\hbar^2}{m}|\langle s|\partial x|x\rangle|^2$, where $|s\rangle$ and $|x\rangle$ are the crystal Bloch functions of the electron in the conduction band and in one of the three p-like degenerate valence bands, respectively. The quantum confinement due to the QD potential breaks the periodicity of the electronic

wave functions, and the derivation of the Roth's formula collapses [57]. Nevertheless, as long as the confinement energy is much smaller than the energies Δ, E_p, and E_g, one still expects Roth's formula to be a qualitative approximation that provides an upper bound on the band gap (a lower bound of the composition x). Indeed, the typical separation between the confined carriers' energy levels in our QD is of order 10–30 meV [58], much smaller than Δ, E_p, and E_g (see Table IV).

Therefore, we proceed by interpolating the values of Δ and E_p using Eq. (55) and the material parameters in Table IV. For the QD band gap, E_g^{QD}, we use the directly measured value of the X_{BE}^0 spectral line, as it takes into account the quantum confinement and lattice mismatch strain effects [59]. To get better estimate for the QD bandgap, however, one has to add to the measured PL the excitonic binding energy. As discussed above, we use the direct Coulomb term J_{ss}^{eh} [Eq. (28)], as an estimate for the excitonic binding energy. Thus $E_g^{\mathrm{QD}} = E^{X_{\mathrm{BE}}^0} + J_{ss}^{eh}$, where $J_{ss}^{eh} \approx 11.3$ meV. The Roth formula for the QD is therefore given by

$$g_e(x) = 2 - \frac{2}{3}\frac{E_p(x)\Delta(x)}{E_g^{\mathrm{QD}}\left[E_g^{\mathrm{QD}} + \Delta(x)\right]}. \tag{57}$$

Using the measured value $g_e(x) = -0.55$ in Eq. (57) and the material parameters from Table IV we get an estimate for the effective QD composition $x = 0.76 \pm 0.04$, where the uncertainty in x includes also the uncertainties in the tabulated band parameters. This value agrees to within the experimental uncertainties with the value obtained from the dielectric constant deduced from the diamagnetic shifts.

D. QD dimensions

One can use the magneto-PL spectroscopy to estimate the QD dimensions. By substituting the measured $\beta_{K_{sp}^{hh}}$ in Eq. (32) one can find the extent of the hole wave function as given by Eq. (18). Using the experimentally estimated $\gamma_0 = 0.976(2)$ the electron wave function extent can be obtained as well. This way we find that l_h and l_e are 11.7(3) and 11.4(3) nm, respectively.

By substituting the measured ratio between the diamagnetic shifts of the hole-hole exchange interaction $\beta_{K_{sp}^{hh}}$ and that of the BE $\beta_{X_{\mathrm{BE}}^0}$ in Eq. (45) we obtain $\chi = 1.36(2)$, which is slightly less than 1.5 expected for a truly 2D exciton. To account for this discrepancy we consider the extent of the excitonic wave function in the z direction l_z. This may be attributed to the fact that the electron mass is isotropic, unlike that of the HH which is much heavier in the z direction [20]. The aspect ratio a between the extent of the BE wave function in the z direction to its extent in the plane is given by $3/\xi - 2 = 0.20(1)$ which leads to $l_z \approx 2.3(1)$ nm.

It follows that the estimated dimensions of the QD are about 23 nm in diameter and 4.5 nm in height. We note that the lateral dimensions are probably underestimated. This is because the confining length of the parabolic potential well model (l_p) is about a factor of 2 smaller than that of an infinite 2D potential well model which produces the same energy difference between the s and p shells of the confined carrier [$\hbar\omega_p$ as defined in Eq. (17)]. The estimated QD height is probably slightly overestimated, due to the penetration of the electronic wave function into the GaAs binary barriers. We note here that the extent of the electronic wave function along the growth direction leads to the following relations between the direct Coulomb terms $|J_{ss}^{ee}| < |J_{ss}^{hh}| \approx |J_{ss}^{eh}|$. These relations leads in turn to the quite general experimental observation that the negatively charged exciton spectral line (X^{-1}) is a few meV lower in energy than the positively charged exciton (X^{+1}) line, while the later is quite close in energy to the neutral exciton line [X_{BE}^0, see Fig. 2(a)].

VI. SUMMARY

We experimentally investigated using polarization sensitive magneto-PL spectroscopy a well-characterized $In_xGa_{1-x}As$ QD in the Faraday configuration. We systematically measured the Zeeman splittings of neutral, singly and doubly charged excitons. The g factors of the bright and dark excitons were measured first and their values were used to show that the Zeeman splittings of various charged excitonic lines can be quite well described by a simple arithmetic model resulting from sums and differences of the g factors of the confined electron and holes in their respective energy levels. In particular, from these measurements we extracted the g factor of the hole in its second confined energy level and showed that it has opposite sign with respect to the hole in its first energy level.

The measured diamagnetic shifts of the excitonic transitions were carefully measured as well. All the transitions showed quadratic dependence on the magnitude of the externally applied magnetic field. In particular, we observed a pronounced negative diamagnetic shift of one of the sptectral lines for transitions from the doubly positively charged excitons ($X_{S_0}^{+2}$). The magneto-PL measurements were all quantitatively explained using a Hartree-Fock model to describe the direct Coloumb and exchange interactions between up to four confined carriers in the QD.

We used a two-dimensional cylindrically symmetric parabolic potential model to analytically calculate the Coulomb and exchange integrals and their magnetic field dependence. The model quantitatively describes the measured diamagnetic shifts of many excitonic transitions and it accurately describes the hole-hole and electron-hole direct Coulomb and exchange interactions and their magnetic field dependence. From our measurements and model we obtained an estimate for the QD average dielectric constant (ϵ_r), and for its lateral dimensions $l_h \approx l_e$. In addition, we show that while the 2D model is adequate for describing the confined heavy hole wave functions, the perpendicular extent of the electron wave function must be considered to quantitatively account for the exciton diamagnetic shift. The latter extent provides an estimate for the QD height, in decent agreement with the structural data at hand. Last, we show that by interpolating both the QD electronic g factor and its dielectric constant between the QD's binary constituents GaAs and InAs we succeed to provide similar estimates for the $In_xGa_{1-x}As$ QD average composition x. Although simple, the model provides a good understanding of the experimental magneto optics of charge-tunable quantum dots.

ACKNOWLEDGMENTS

We thank Dr. J. Tilchin, and Prof. E. Lifshitz for their help, and Prof. M. M. Glazov and Prof. E. L. Ivchenko for valuable discussions. The support of the Israeli Science Foundation (ISF), Grant No. 1933/23 and that of the German Israeli Research Cooperation (DIP) (DFG: Grant No. FI 947/6-1) are gratefully acknowledged.

[1] E. Dekel, D. Gershoni, E. Ehrenfreund, J. M. Garcia, and P. M. Petroff, Carrier-carrier correlations in an optically excited single semiconductor quantum dot, Phys. Rev. B **61**, 11009 (2000).

[2] P. Michler, A. Kiraz, C. Becher, W. V. Schoenfeld, P. M. Petroff, L. Zhang, E. Hu, and A. Imamoglu, A quantum dot single-photon turnstile device, Science **290**, 2282 (2000).

[3] N. Tomm, A. Javadi, N. O. Antoniadis, D. Najer, M. C. Loebl, A. R. Korsch, R. Schott, S. R. Valentin, A. D. Wieck, A. Ludwig, and R. J. Warburton, A bright and fast source of coherent single photons, Nat. Nanotechnol. **16**, 399 (2021).

[4] C. Santori, M. Pelton, G. Solomon, Y. Dale, and Y. Yamamoto, Triggered single photons from a quantum dot, Phys. Rev. Lett. **86**, 1502 (2001).

[5] C. Lu and J. Pan, Quantum-dot single-photon sources for the quantum internet, Nat. Nanotechnol. **16**, 1294 (2021).

[6] D. Cogan, G. Peniakov, O. Kenneth, Y. Don, and D. Gershoni, Quantum tomography of entangled spin-multiphoton states, Phys. Rev. Appl. **18**, 024055 (2022).

[7] J. Berezovsky, M. H. Mikkelsen, N. G. Stoltz, L. A. Coldren, and D. D. Awschalom, Picosecond coherent optical manipulation of a single electron spin in a quantum dot, Science **320**, 349 (2008).

[8] D. Press, T. D. Ladd, B. Zhang, and Y. Yamamoto, Complete quantum control of a single quantum dot spin using ultrafast optical pulses, Nature (London) **456**, 218 (2008).

[9] Y. Kodriano, I. Schwartz, E. Poem, Y. Benny, R. Presman, T. A. Truong, P. M. Petroff, and D. Gershoni, Complete control of a matter qubit using a single picosecond laser pulse, Phys. Rev. B **85**, 241304(R) (2012).

[10] I. Schwartz, E. R. Schmidgall, L. Gantz, D. Cogan, E. Bordo, Y. Don, M. Zielinski, and D. Gershoni, Deterministic writing and control of the dark exciton spin using single short optical pulses, Phys. Rev. X **5**, 011009 (2015).

[11] N. Akopian, N. H. Lindner, E. Poem, Y. Berlatzky, J. Avron, D. Gershoni, B. D. Gerardot, and P. M. Petroff, Entangled photon pairs from semiconductor quantum dots, Phys. Rev. Lett. **96**, 130501 (2006).

[12] E. Togan, Y. Chu, A. S. Trifonov, L. Jiang, J. Maze, L. Childress, M. V. G. Dutt, A. S. Sørensen, P. R. Hemmer, A. S. Zibrov, and M. D. Lukin, Quantum entanglement between an optical photon and a solid-state spin qubit, Nature (London) **466**, 730 (2010).

[13] M. Ghali, K. Ohtani, Y. Ohno, and H. Ohno, Generation and control of polarization-entangled photons from GaAs island quantum dots by an electric field, Nat. Commun. **3**, 661 (2012).

[14] W. B. Gao, P. Fallahi, E. Togan, J. Miguel-Sanchez, and A. Imamoglu, Observation of entanglement between a quantum dot spin and a single photon, Nature (London) **491**, 426 (2012).

[15] K. De Greve, L. Yu, P. L. McMahon, J. S. Pelc, C. M. Natarajan, N. Y. Kim, E. Abe, S. Maier, C. Schneider, M. Kamp, S. Hoefling, R. H. Hadfield, A. Forchel, M. M. Fejer, and Y. Yamamoto, Quantum-dot spin-photon entanglement via frequency downconversion to telecom wavelength, Nature (London) **491**, 421 (2012).

[16] J. R. Schaibley, A. P. Burgers, G. A. McCracken, L.-M. Duan, P. R. Berman, D. G. Steel, A. S. Bracker, D. Gammon, and L. J. Sham, Demonstration of quantum entanglement between a single electron spin confined to an InAs quantum dot and a photon, Phys. Rev. Lett. **110**, 167401 (2013).

[17] I. Schwartz, D. Cogan, E. R. Schmidgall, Y. Don, L. Gantz, O. Kenneth, N. H. Lindner, and D. Gershoni, Deterministic generation of a cluster state of entangled photons, Science **354**, 434 (2016).

[18] G. Peniakov, Z.-E. Su, A. Beck, D. Cogan, O. Amar, and D. Gershoni, Towards supersensitive optical phase measurement using a deterministic source of entangled multiphoton states, Phys. Rev. B **101**, 245406 (2020).

[19] D. Cogan, Z.-E. Su, O. Kenneth, and D. Gershoni, Deterministic generation of indistinguishable photons in a cluster state, Nat. Photon. **17**, 324 (2023).

[20] E. L. Ivchenko, *Optical Spectroscopy of Semiconductor Nanostructures* (Alpha Science, Oxford, UK, 2005).

[21] Y. J. Fu, S. D. Lin, M. F. Tsai, H. Lin, C. H. Lin, H. Y. Chou, S. J. Cheng, and W. H. Chang, Anomalous diamagnetic shift for negative trions in single semiconductor quantum dots, Phys. Rev. B **81**, 113307 (2010).

[22] M. M. Glazov, E. L. Ivchenko, O. Krebs, K. Kowalik, and P. Voisin, Diamagnetic contribution to the effect of in-plane magnetic field on a quantum-dot exciton fine structure, Phys. Rev. B **76**, 193313 (2007).

[23] Y. H. Shin, B. K. Choi, Y. Kim, J. D. Song, D. Nakamura, Y. H. Matsuda, and S. Takeyama, Anomalous diamagnetic shifts in InP-GaP lateral quantum-wires, Opt. Express **23**, 28349 (2015).

[24] S. N. Walck and T. L. Reinecke, Exciton diamagnetic shift in semiconductor nanostructures, Phys. Rev. B **57**, 9088 (1998).

[25] C. Schulhauser, D. Haft, R. J. Warburton, K. Karrai, A. O. Govorov, A. V. Kalameitsev, A. Chaplik, W. Schoenfeld, J. M. Garcia, and P. M. Petroff, Magneto-optical properties of charged excitons in quantum dots, Phys. Rev. B **66**, 193303 (2002).

[26] Y. Benny, Y. Kodriano, E. Poem, D. Gershoni, T. A. Truong, and P. M. Petroff, Excitation spectroscopy of single quantum dots at tunable positive, neutral, and negative charge states, Phys. Rev. B **86**, 085306 (2012).

[27] M. Zielinski, Y. Don, and D. Gershoni, Atomistic theory of dark excitons in self-assembled quantum dots of reduced symmetry, Phys. Rev. B **91**, 085403 (2015).

[28] Certain commercial equipment, instruments, software, or materials are identified in this paper to specify the procedures or equipment used. Such identification is not intended to imply recommendation or endorsement by the National Institute of Standards and Technology, nor is it intended to imply that the materials, equipment or software identified are necessarily the best available for the purpose.

[29] E. Poem, J. Shemesh, I. Marderfeld, D. Galushko, N. Akopian, D. Gershoni, B. D. Gerardot, A. Badolato, and P. M. Petroff, Polarization sensitive spectroscopy of charged quantum dots, Phys. Rev. B **76**, 235304 (2007).

[30] Y. Benny, S. Khatsevich, Y. Kodriano, E. Poem, R. Presman, D. Galushko, P. M. Petroff, and D. Gershoni, Coherent optical writing and reading of the exciton spin state in single quantum dots, Phys. Rev. Lett. **106**, 040504 (2011).

[31] I. Schwartz, D. Cogan, E. R. Schmidgall, L. Gantz, Y. Don, M. Zielinski, and D. Gershoni, Deterministic coherent writing of a long-lived semiconductor spin qubit using one ultrafast optical pulse, Phys. Rev. B **92**, 201201(R) (2015).

[32] Y. Don, M. Zielinski, and D. Gershoni, The optical activity of the dark exciton, arXiv:1601.05530.

[33] Y. Kodriano, E. R. Schmidgall, Y. Benny, and D. Gershoni, Optical control of single excitons in semiconductor quantum dots, Semicond. Sci. Technol. **29**, 053001 (2014).

[34] M. Bayer, G. Ortner, O. Stern, A. Kuther, A. A. Gorbunov, A. Forchel, P. Hawrylak, S. Fafard, K. Hinzer, T. L. Reinecke, S. N. Walck, J. P. Reithmaier, F. Klopf, and F. Schafer, Fine structure of neutral and charged excitons in self-assembled In(Ga)As/(Al)GaAs quantum dots, Phys. Rev. B **65**, 195315 (2002).

[35] P. Y. Yu and M. Cardona, *Fundamentals of Semiconductors* (Springer, Berlin, 2010).

[36] B. J. Witek, R. W. Heeres, U. Perinetti, E. P. A. M. Bakkers, L. P. Kouwenhoven, and V. Zwiller, Measurement of theg-factor tensor in a quantum dot and disentanglement of exciton spins, Phys. Rev. B **84**, 195305 (2011).

[37] M. Bayer, A. Kuther, A. Forchel, A. Gorbunov, V. B. Timofeev, F. Schäfer, J. P. Reithmaier, T. L. Reinecke, and S. N. Walck, Electron and hole *g* factors and exchange interaction from studies of the exciton fine structure in $In_{0.60}Ga_{0.40}As$ quantum dots, Phys. Rev. Lett. **82**, 1748 (1999).

[38] J. G. Tischler, A. S. Bracker, D. Gammon, and D. Park, Fine structure of trions and excitons in single GaAs quantum dots, Phys. Rev. B **66**, 081310(R) (2002).

[39] L. Gantz, E. R. Schmidgall, I. Schwartz, Y. Don, E. Waks, G. Bahir, and D. Gershoni, Controlling the dark exciton spin eigenstates by external magnetic field, Phys. Rev. B **94**, 045426 (2016).

[40] E. R. Schmidgall, I. Schwartz, D. Cogan, L. Gantz, Y. Don, and D. Gershoni, Coherent Control of Dark Excitons in Semiconductor Quantum Dots, in *Quantum Dots for Quantum Information Technologies*, edited by P. Michler (Springer International Publishing, Cham, Switzerland, 2017), pp. 123–164.

[41] Y. Kodriano, E. Poem, N. H. Lindner, C. Tradonsky, B. D. Gerardot, P. M. Petroff, J. E. Avron, and D. Gershoni, Radiative cascade from quantum dot metastable spin-blockaded biexciton, Phys. Rev. B **82**, 155329 (2010).

[42] G. Peniakov, Magneto-optical study of semiconductor quantum dots, Master's thesis, Technion—The Israeli Institute of Technology, 2017.

[43] A. Beck, Magneto optic studies of quantum dot confined charge carriers and excitons, Master's thesis, Technion—The Israeli Institute of Technology, 2020.

[44] A. Kiselev, E. Ivchenko, A. Sirenko, T. Ruf, M. Cardona, D. Yakovlev, W. Ossau, A. Waag, and G. Landwehr, Electron and hole *g* factor anisotropy in CdTe/CdMgTe quantum wells, J. Cryst. Growth **184–185**, 831 (1998).

[45] C. C. J. Roothaan, New developments in molecular orbital theory, Rev. Mod. Phys. **23**, 69 (1951).

[46] T. Takagahara, Theory of exciton doublet structures and polarization relaxation in single quantum dots, Phys. Rev. B **62**, 16840 (2000).

[47] E. Kadantsev and P. Hawrylak, Theory of exciton fine structure in semiconductor quantum dots: Quantum dot anisotropy and lateral electric field, Phys. Rev. B **81**, 045311 (2010).

[48] R. J. Warburton, B. T. Miller, C. S. Durr, C. Bodefeld, K. Karrai, J. P. Kotthaus, G. Medeiros-Ribeiro, P. M. Petroff, and S. Huant, Coulomb interactions in small charge-tunable quantum dots: A simple model, Phys. Rev. B **58**, 16221 (1998).

[49] S. Taguchi, T. Goto, M. Takeda, and G. Kido, Magneto-optical effects of the Wannier exciton in biaxial ZnP_2 crystal, J. Phys. Soc. Jpn. **57**, 3256 (1988).

[50] M. Bayer, S. N. Walck, T. L. Reinecke, and A. Forchel, Exciton binding energies and diamagnetic shifts in semiconductor quantum wires and quantum dots, Phys. Rev. B **57**, 6584 (1998).

[51] M. Ediger, G. Bester, B. D. Gerardot, A. Badolato, P. M. Petroff, K. Karrai, A. Zunger, and R. J. Warburton, Fine structure of negatively and positively charged excitons in semiconductor quantum dots: Electron-hole asymmetry, Phys. Rev. Lett. **98**, 036808 (2007).

[52] D. V. Regelman, E. Dekel, D. Gershoni, E. Ehrenfreund, A. J. Williamson, J. Shumway, A. Zunger, W. V. Schoenfeld, and P. M. Petroff, Optical spectroscopy of single quantum dots at tunable positive, neutral, and negative charge states, Phys. Rev. B **64**, 165301 (2001).

[53] S. Adachi, Gallium arsenide (GaAs), in *Optical Constants of Crystalline and Amorphous Semiconductors: Numerical Data and Graphical Information* (Springer US, Boston, MA, 1999), pp. 213–226.

[54] Y. A. Goldberg and N. M. Schmidt, Gallium Indium Arsenide, in *Handbook Series on Semiconductor Parameters*, Vol. 2, edited by M. Levinshtein, S. Rumyantsev, and M. Shur (World Scientific, London, UK, 1999), pp. 62–88.

[55] I. Vurgaftman, J. R. Meyer, and L. R. Ram-Mohan, Band parameters for III–V compound semiconductors and their alloys, J. Appl. Phys. **89**, 5815 (2001).

[56] L. M. Roth, B. Lax, and S. Zwerdling, Theory of optical magneto-absorption effects in semiconductors, Phys. Rev. **114**, 90 (1959).

[57] C. E. Pryor and M. E. Flatté, Landé *g* factors and orbital momentum quenching in semiconductor quantum dots, Phys. Rev. Lett. **96**, 026804 (2006).

[58] Y. Benny, Y. Kodriano, E. Poem, S. Khatsevitch, D. Gershoni, and P. M. Petroff, Two-photon photoluminescence excitation spectroscopy of single quantum dots, Phys. Rev. B **84**, 075473 (2011).

[59] J. van Bree, A. Y. Silov, P. M. Koenraad, M. E. Flatte, and C. E. Pryor, *g*-factors and diamagnetic coefficients of electrons, holes, and excitons in InAs/InP quantum dots, Phys. Rev. B **85**, 165323 (2012).